


Interpolating climate variables by using INLA and the SPDE approach

Guido Fioravanti^{1,2}  | Sara Martino³ | Michela Cameletti⁴ | Andrea Toreti¹

¹European Commission, Joint Research Centre, Ispra, Italy

²VAL-CLO, ISPRA, Rome, Italy

³Norwegian University of Science and Technology, Trondheim, Norway

⁴Department of Economics, University of Bergamo, Bergamo, Italy

Correspondence

Guido Fioravanti, European Commission, Joint Research Centre (JRC), Via E. Fermi 2749, 21027 Ispra, Italy.

Email: guido.fioravanti@ec.europa.eu

Abstract

Gridded observational products of the main climate parameters are essential in climate science. Current interpolation approaches, implemented to derive such products, often lack of a proper uncertainty propagation and representation. In this study, we introduce a Bayesian spatiotemporal approach based on the integrated nested Laplace approximation (INLA) and the stochastic partial differential equation (SPDE). The method is described and discussed by using a real case study based on high-resolution monthly 2-m maximum (Tmax) and minimum (Tmin) air temperature over Italy in 1961–2020. The INLA-SPDE based approach is able to properly take into account uncertainties in the final gridded products and offers interesting promising advantages to deal with non-stationary and non-Gaussian multisource data.

KEYWORDS

Bayesian approach, INLA, spatiotemporal correlation, SPDE, temperature climatology, uncertainty

1 | INTRODUCTION

Near-surface 2-m air temperature (hereafter T_a) provides essential information on the state of the climate system, its variability, extremes and its changes (Fang et al., 2022; Lian et al., 2017). It is easily understandable and it can be used for communicating effectively climate science and climate change to the general public. Thus, it should not come as a surprise that T_a plays an important role as a target of the Paris agreement and, more generally, for climate change related political processes (GCOS, 2017).

While the Sixth Assessment Report (AR6) of the IPCC (Masson-Delmotte et al., 2021) emphasizes that climate change will induce a general increase in the frequency and intensity of extreme events (such as heatwaves, heavy precipitation, droughts), it has to be noted that global warming is not homogeneous throughout the

globe and some areas are seeing a faster rate of warming than others (Rantanen et al., 2022; Zittis et al., 2022). The Mediterranean area is a notable example of this fact (Tuel & Eltahir, 2020). Observational records and model-based studies clearly indicate the Mediterranean as a prominent climate change hot-spot, with a rate of warming which has accelerated particularly after the 1980s and is higher than the global average (Bruley et al., 2022; Cos et al., 2022; Lionello & Scarascia, 2018; Pastor et al., 2020; Zittis et al., 2019). Italy, located in the very middle of the Mediterranean basin, is particularly exposed to climate change impacts especially in the south where a considerable number of municipalities show low levels of resilience to disasters (Spano et al., 2020).

The collection and analysis of observational records from meteorological ground weather stations provides essential information for analysing past and current

This is an open access article under the terms of the [Creative Commons Attribution](https://creativecommons.org/licenses/by/4.0/) License, which permits use, distribution and reproduction in any medium, provided the original work is properly cited.

© 2023 The Authors. *International Journal of Climatology* published by John Wiley & Sons Ltd on behalf of Royal Meteorological Society.

trend, variability, as well as possible future climate scenarios. When interpolated into a regular grid, observational sparse data find use in a variety of scientific and operational applications such as statistical downscaling of Earth System Models and development of bias-adjusted climate change scenarios (Herrera et al., 2019; Tarek et al., 2021).

In recent decades, a number of gridded climate products has been produced. A selected collection of these products at the European (e.g., E-OBS) and global scale (e.g., CRU, GISTEMP, Berkeley Earth) is available through the Copernicus Climate Change Service (<https://doi.org/10.24381/cds.11dedf0c>). A review of the E-OBS dataset and its applications is available, among others, in Cornes et al. (2018), Ledesma and Futter (2017) and Raymond et al. (2017), while an example of evaluation of the accuracy of the E-OBS dataset against local observational measurements in Italy (Apulia region) can be found in My et al. (2022).

Several interpolation techniques are available to produce gridded maps from scattered in situ measurements of climate variables (Chen & Guo, 2017; Hofstra et al., 2008; Yang & Xing, 2021) and most of them are implemented in software packages for the R language (R Core Team, 2021). For example, *gstat* (Pebesma, 2004) is a well-known and user-friendly R package which implements both deterministic (inverse distance weighting [IDW]) and geostatistical (traditional kriging and its variants) methods. Geostatistical methods assume that the observed data are a realization of a continuously indexed spatial random field (Gelfand et al., 2010). In this respect, Gaussian random fields (GRFs) play a dominant role in spatial statistics and especially in the traditional field of geostatistics (Lindgren et al., 2011). Conversely, for deterministic methods no probabilistic model of data generation is taken into account. While geostatistical methods allow to attach an uncertainty measure to the individual spatial predictions, with deterministic methods is only possible to calculate an overall error rate (e.g., the root-mean-square error) by doing cross-validation (Sahu, 2021).

Uncertainty estimate is an important aspect to be considered when selecting and/or developing interpolation methods. Despite climate records not being immune to measurement and modelling uncertainties, scientists and practitioners typically have to deal with datasets for which the uncertainty information is generic, misleading, or absent (Merchant et al., 2017). Indeed, the available gridded datasets typically provide a single estimate for each specific location and time step (Tang et al., 2022), where a measure of uncertainty (the degree to which something is known; Nature, 2019) would allow to assess reliability and effects on derived products and information.

Although classical kriging is a very popular geostatistical method among climate practitioners, it is often neglected that its estimates of the prediction

variance do not account for the uncertainty caused by inferring the covariance parameters from the data (Moyeed & Papritz, 2002; Pilz et al., 2005). In other words, by assuming that the spatial covariance function is known (Handcock & Stein, 1993; Helbert et al., 2009; Song et al., 2015) classical kriging suffers from uncertainty underestimation.

Concerning Italy, several exercises have been recently done and several products made available. For instance, Crespi et al. (2021) used a combination of two deterministic methods (IDW and PRISM; Daly et al., 2002) to develop high-resolution gridded datasets of daily mean temperature and precipitation records during 1980–2018 in northeastern Italy (Trentino-South Tyrol region). IDW was also applied in Caloiero et al. (2020) for southern Italy (Calabria region). Curci et al. (2021) employed a geostatistical approach (universal kriging) to generate interpolated maps for mean temperature and precipitation in central Italy (Abruzzo region) over the period 1930–2019. A comparison of IDW and geostatistical methods to produce monthly gridded precipitation over southern Italy (Calabria region) is discussed in Pellicone et al. (2018). Finally, Brunetti et al. (2014) applied regression analysis (local weighted linear regression [LWLR]) to obtain 1961–1990 monthly temperature climatologies for Italy. Although Brunetti et al. provide examples of uncertainty estimates (68% confidence interval) associated to each grid point, the proposed LWLR method does not explicitly account for the autocorrelation of data. Indeed, that method consists in an iterative application of local temperature-versus-elevation weighted regressions where the stations which contribute to the temperature estimates are searched within an a priori fixed spatial range of 200 km from a given grid cell.

In this study, we use a spatiotemporal regression model to interpolate T_{max} and T_{min} monthly mean data on a large space–time domain, namely the entire Italian territory for 60 years (1961–2020). We develop the statistical analysis in a Bayesian framework in order to incorporate all reasonable sources of uncertainty (including the parameters of the covariance function) in the final inferential summaries. Because of the large space–time domain, the inferential analysis has been implemented using the integrated nested Laplace approximation (INLA) approach (Rue et al., 2009) and the spatiotemporal covariance function has been derived from the solution of a stochastic partial differential equation (SPDE; Lindgren & Rue, 2015).

INLA is a deterministic algorithm which provides accurate approximation of the marginal posterior distributions of the model parameters based on Laplace and other numerical approximations and integration schemes. The SPDE approach provides a way to represent a continuous Gaussian Random Field through a

discretely indexed Gaussian Markov random field (GMRF; Lindgren et al., 2011). Computationally, GMRFs are much more efficient than GRFs as they are based on sparse matrices. The INLA-SPDE approach has been proved to be computationally faster than the simulation-based Markov chain Monte Carlo (MCMC) approach commonly used for Bayesian inference (Martino & Riebler, 2020). This is fundamental when models are complex or deal with massive datasets (Blangiardo & Cameletti, 2015).

The effective use of INLA and SPDE is documented in several studies based on environmental data, from ecological applications to disease mapping. A comprehensive list of updated references is available in Lindgren et al. (2022). Going through this list, it is illuminating to note the absence of applications in climate science. To bridge this gap, we here introduce INLA and SPDE by using and discussing a simple case study. In particular, we employ INLA and SPDE to develop a spatiotemporal model to derive gridded monthly temperature climatologies for Italy both for the most recent standard 30-year period (1991–2020) and three previous standard periods (1961–1990, 1971–2000, 1981–2010).

The input dataset is described in section 2. Section 3 introduces the statistical model, while section 4 discusses results, model validation and possible applications of the model estimates. Section 5 reviews the benefits of the INLA/SPDE approach.

2 | DATA

2.1 | The study area

Italy, with latitude boundaries between 36°N and 48°N and longitude boundaries between 5°E and 20°E, is our study domain. The country is characterized by a narrow and long shape of about 7500 km of coast line which extends into the Mediterranean sea, two large mountain systems (the Alps to the north, and the Apennines which run northwest to south along the country), a large plain (the Po Valley with a surface of 46,000 km²) and two major islands (Sicily and Sardinia). This complex morphology leads to variegated and contrasted climate regimes (from warm temperate with dry summer to polar) which strongly influences the variability of soil moisture and temperature (Lo Papa et al., 2020).

According to the technical report “Climate indicators in Italy” (ISPRA, 2021), which uses a dataset of 140 homogenized daily temperature time series from 1961 to 2020, the Italian-average mean-temperature anomalies (baseline period 1961–1990) are generally characterized by higher variability than global anomalies. The estimated warming trend for the annual Tmax and

Tmin Italian averages is +0.42 and +0.35°C·decade⁻¹, respectively. As regards Tmax, a positive anomaly of +1.82°C ranks 2020 as the warmest year in Italy since 1961 (2021 and 2022 are not included in this analysis).

2.2 | Temperature data

Our study uses daily maximum and minimum temperature records taken from SCIA (Desiato et al., 2011), a database which collects climate observations from a national network (the Italian Air Force synoptic network) and several meteorological, agro-meteorological and hydrographic networks across the 20 Italian regions. In SCIA, the raw temperature data are subjected to strict quality controls (ISPRA, 2016) for the detection of erroneous daily observations. Such quality controls are basically a subset of those described by Durre et al. (2010) for the Global Historical Climatology Network (GHCN) dataset (Menne et al., 2012).

Despite the large number of temperature records which populate the SCIA database, here, we only focus on those time series which supply data during 1961–2020 and with no missing data for the 2011–2020 decade. This choice is motivated by the fact that the 2011–2020 decade was particularly remarkable as regards global warming, being the warmest on record since 1961 both in Italy and at global scale (ISPRA, 2021; WMO, 2021).

The altitude of the selected weather stations varies between 0 (Villapiana Scalo, Marina di Ravenna, Fossalon stations) and 3488 m (Pian Rosa station) above mean sea level. Figure 1 displays their spatial distribution, while the inset on the left shows the number of available stations across the years. A visual inspection reveals that only a limited number of stations provides a complete coverage of the study period. Specifically, less than 250 stations are available over the first 30 years (1961–1990), while more than 500 stations are available since the early 2000s. This increase in the station number corresponds to the development of local hydrographic authorities and regional environmental agencies in Italy and the transition from mechanical to automatic station networks (Libertino et al., 2018).

The homogenization of temperature time series is a pre-requisite for applying statistical data analysis (Toreti et al., 2011). For the detection and adjustment of nonclimate perturbations (breakpoints) in temperature time series we used Climatol (Guijarro, 2019), a ready-to-use R package and an automatic well-established homogenization tool (Joelsson et al., 2022). Details and results of the homogenization study are not given here for lack of space. We refer interested readers to Fioravanti et al. (2019) for a more in-depth description both of the continuity and completeness criteria adopted for the selection

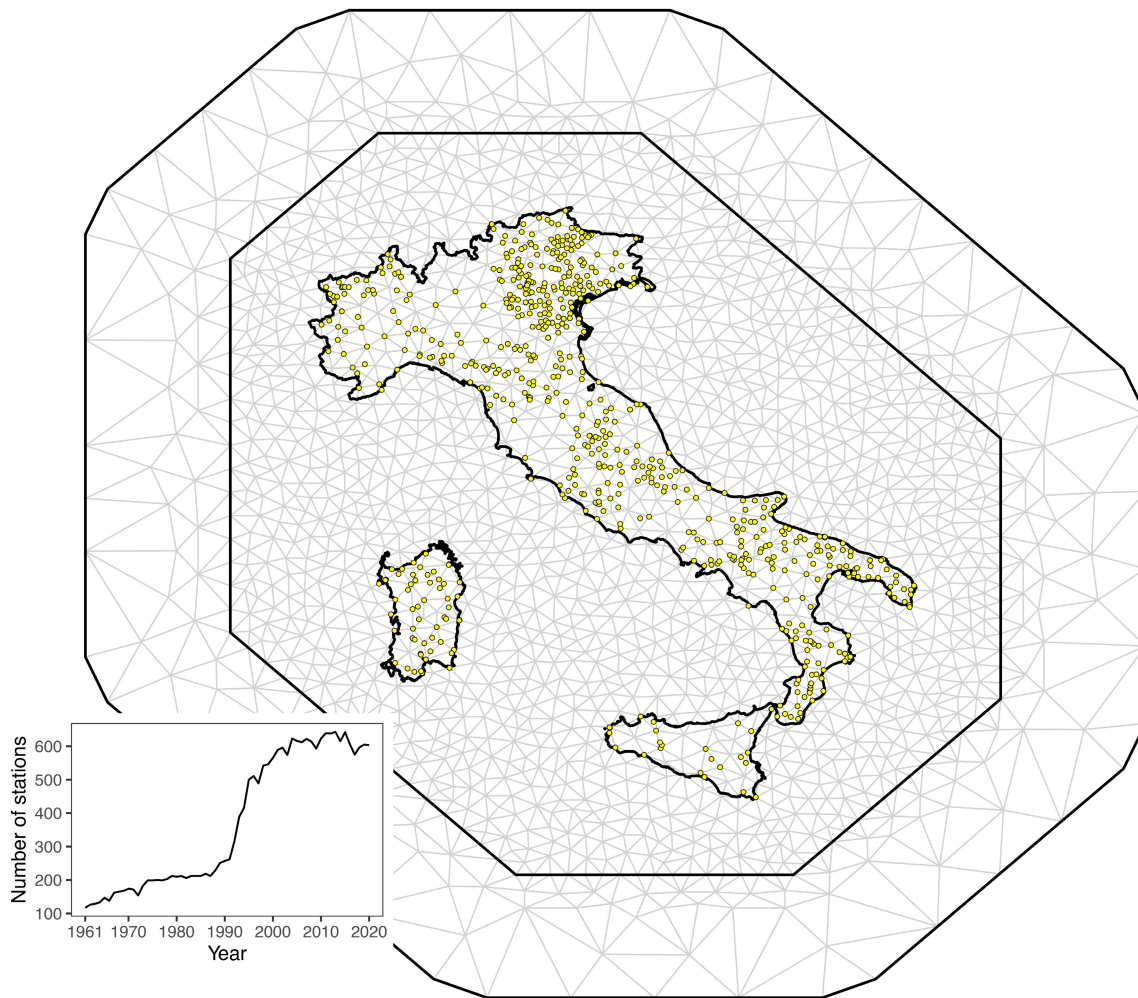


FIGURE 1 Spatial distribution and historical time series (inset, bottom-left) of the number of the selected input stations for the month of June (Tmax). The same results hold for Tmin and the other months of the year. In the background, the mesh used to build the SPDE approximation to the continuous Matérn field. Note, our study domain comprises only the Italian peninsula and the two major islands (Sicily and Sardinia) [Colour figure can be viewed at [wileyonlinelibrary.com](https://onlinelibrary.wiley.com/terms-and-conditions)]

of the temperature time series and the homogenization process.

Tmax and Tmin monthly averages were calculated using only daily observations collected during the 1961–2020 period, no estimation or smoothing methods were applied to refill data gaps. The daily data were averaged by month for each year following the “10/4” completeness rule (WMO, 2017), which states that monthly values should not be calculated when (1) observations are missing for 11 or more days during the month; (2) observations are missing for a period of 5 or more consecutive days during the month.

2.3 | Terrain and location predictors

We used the following variables as predictors of the Tmax and Tmin monthly mean temperatures: latitude, elevation

and distance to sea (Osborn et al., 2021). All these predictors have a clear and physically sound effect on air temperature.

For interpolation purposes, the predictors must be available as rectangular raster datasets (see Figure 2). The latitude raster simply contains the latitude value (Universal Transversal Mercator original coordinates scaled to kilometres) for each grid cell. The “distance to sea” raster contains the minimum Euclidean distance of each grid point to the Italian coastline. These two rasters were generated by using the geoprocessing capabilities of the R terra package (Maechler et al., 2021). Finally, the digital elevation model dataset EU-DEM v1.1 from the Land Monitoring Service of Copernicus (<https://land.copernicus.eu/imagery-in-situ/eu-dem>) was used as the elevation raster. The final spatial resolutions of the gridded predictors is 1 km × 1 km.

All these predictors have been rescaled to have zero mean and standard deviation equal to one to avoid

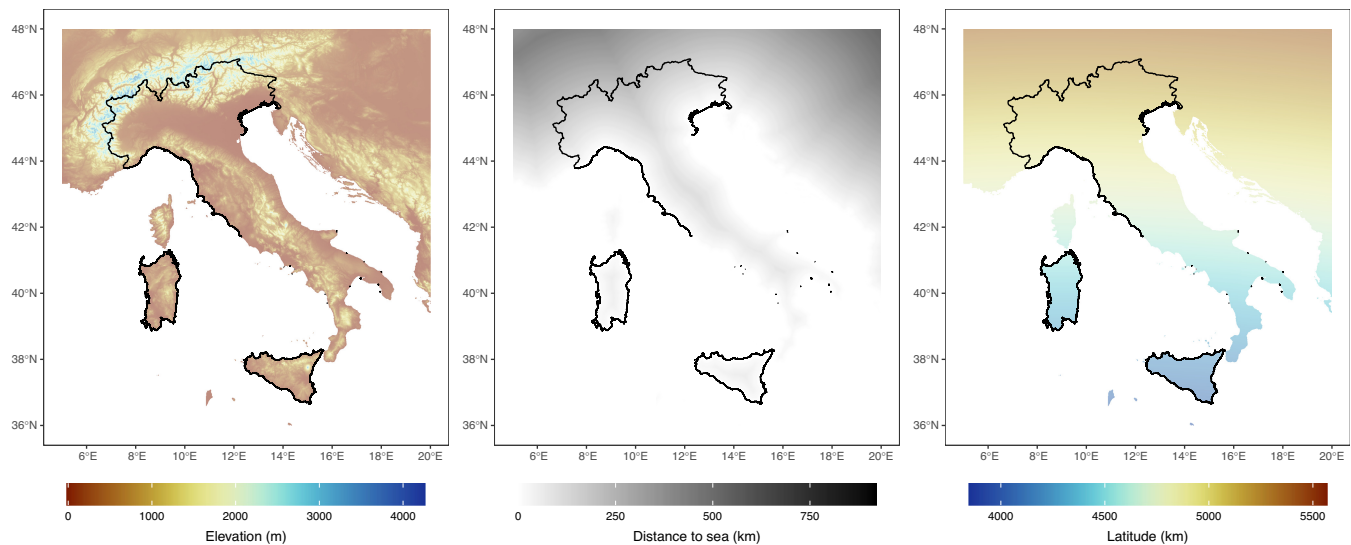


FIGURE 2 Raster maps of the spatial predictors used for interpolating Tmax and Tmin monthly mean records over the period 1961–2020 [Colour figure can be viewed at [wileyonlinelibrary.com](https://onlinelibrary.wiley.com/doi/10.1002/joc.8240)]

numerical problems and ease interpretability of their effects on temperature data.

3 | METHODOLOGY

3.1 | Modelling monthly temperatures with INLA and the SPDE

Here, we introduce the mathematics which defines our statistical model. Before that, we clearly motivate why an explicit spatiotemporal approach is needed: to this end, we start from a simple regression model.

Let $y^m(t, s)$ denote the realization of a space–time process $Y^m(t, s)$ which represents the monthly Tmax (Tmin) mean temperatures at year $t=1961, \dots, 2020$ of month $m=1, \dots, 12$ at location $s \in \mathcal{S}$, where \mathcal{S} is the domain of interest. A linear model where the covariates account for the temporal and spatial trend can be written as

$$y^m(t, s) = \mu^m + \alpha^m t + \mathbf{x}(s)\beta^{mT} + \varepsilon^m(t, s). \quad (1)$$

Here μ^m is a month specific intercept, $\mathbf{x}(s)$ is the vector of observed covariates (introduced in section 2.3), β^m is the vector of coefficients to be estimated. We also include a linear time trend with coefficient α^m and a Gaussian distributed independent measurement error $\varepsilon^m(t, s)$ with mean 0 and standard deviation σ_ε^m . We fit the same model independently for each month and for both Tmax and Tmin (24 models in total), as from our exploratory analysis (not shown) we observed that the impact of each predictor varies across months. As we

are interested in the long term trend for each month, modelling each months' time series independently considerably simplifies the model allowing to ignore the seasonal cycle of temperatures and the strong temporal dependence between consecutive months. To ease the notation in the rest of the paper we omit the month index m .

We fit a simple multiple linear regression model in Equation (1) to our data and, only for exploratory purposes, use spatiotemporal variograms (Wikle et al., 2019) to investigate the independence assumption in model residuals $\varepsilon(t, s)$.

Figure 3 shows the variograms for the residuals of model 1 (solid lines) for all the 12 months fitted with Tmax data (similar results hold for Tmin, not shown). Spatial correlation is clearly visible in all panels, moreover, the variograms show that the residual spatial correlation varies across months. For example, September and October are characterized by large range spatial dependence with the variance increasing slowly, while December and January are characterized by a clear spatial range of 150 km. When it comes to time, all months exhibit week temporal correlation. In summary, the results of Figure 3 indicate that the standard assumption of independent and identically distributed errors is not tenable for our dataset. For a more general review of potential pitfalls that can seriously affect the results of ordinary least square regression we suggest Zuur et al. (2010).

We therefore modify the model including random effects terms that explicitly account for spatial and temporal correlation among temperature records,

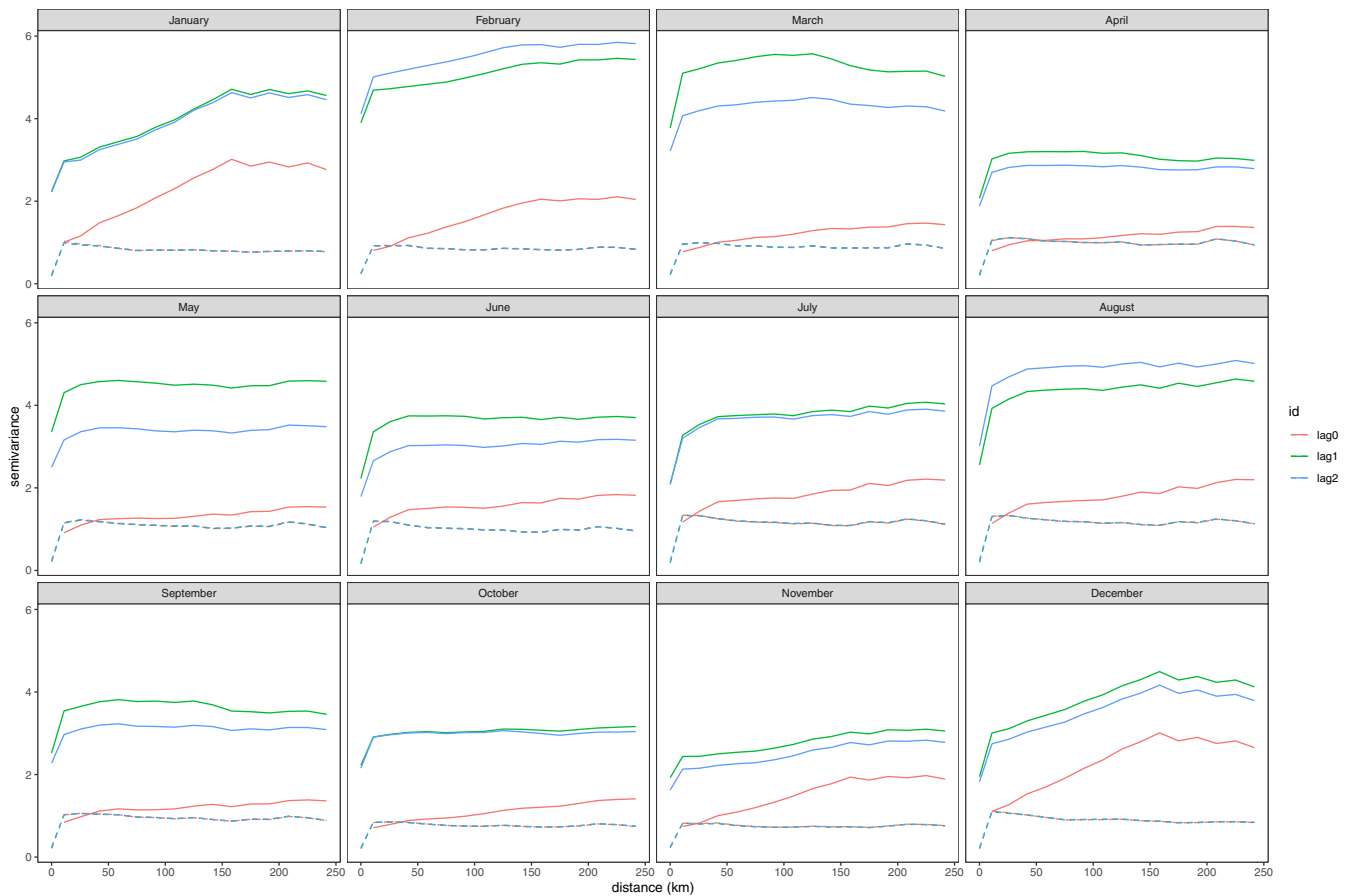


FIGURE 3 Monthly spatiotemporal variograms for the residuals of the linear model in Equation (1) (solid lines) and the spatiotemporal model in Equation (2) (dashed lines). Results refer to the Tmax parameter. Similar results hold for Tmin [Colour figure can be viewed at [wileyonlinelibrary.com](https://onlinelibrary.wiley.com/doi/10.1002/joc.8240)]

$$y(t,s) = \mu + \alpha t + \mathbf{x}(s)\beta' + \omega(t,s) + z(t) + \varepsilon(t,s). \quad (2)$$

Here, $z(t) \sim \mathcal{N}(0, \sigma_z^2)$, $t=1961, \dots, 2020$, is a temporal random effect meant to account for the extra temporal variability (colder or warmer than average years) that is not captured by the linear time trend. A similar effect is used in Serrano-Notivol et al. (2019) for the estimation of daily temperatures in Spain.

The term $\omega(t,s)$ is a spatially correlated process meant to capture the residual dependence beside that described by the covariates. We assume $\omega(t,s)$ to be independent in time but correlated in space with covariance function,

$$\text{Cov}(\omega(t,s), \omega(t',s')) = \begin{cases} 0, & \text{for } t \neq t' \\ \mathcal{C}(h), & \text{for } t = t' \end{cases}, \quad (3)$$

where $h = \|s - s'\|$ is the Euclidean distance between sites s and s' .

A common specification for the purely spatial covariance function $\mathcal{C}(h)$ is the Matérn function,

$$\mathcal{C}(h) = \sigma_\omega^2 \frac{1}{\Gamma(\nu) 2^{\nu-1}} (k h)^\nu K_\nu(k h), \quad (4)$$

where σ_ω^2 is the marginal variance and $K_\nu(\cdot)$ the Bessel function of second kind and order $\nu > 0$. The parameter ν measures the degree of spatial smoothness of the process. As this parameter is hard to estimate, we fixed it to one as suggested by Blangiardo and Cameletti (2015). The term $k > 0$ is a scaling parameter related to the range ρ , that is, the distance at which the spatial correlation becomes negligible (close to 0.1). The larger ρ is, the more dependent the spatial process is. In Equation (4) ρ is defined as $\frac{\sqrt{8\nu}}{k}$, an empirically derived definition proposed by Lindgren et al. (2011). To represent the continuous field $\omega(t,s)$ as a GMRF, we used the SPDE approach, which is based on the finite element method (fem). In our case, the triangulation used for fem is the one shown in Figure 1. In order to obtain accurate approximations of the underlying GRF, the triangular mesh must be dense enough to capture the spatial variability of the monthly mean temperatures. It is noteworthy to observe that we

constructed a mesh which is rather dense over the study domain and sparser in the outer region. The purpose of the outer region is twofold: avoid boundary effects and, at the same time, reduce the computational costs.

3.2 | Priors definition

We finalize our Bayesian model by defining priors on all model parameters: the coefficients α and β , the standard deviations $\sigma_\varepsilon, \sigma_z, \sigma_\omega$ and the range ρ of the Matérn function. We used vague independent Gaussian priors for α and β and log-Gamma priors on the log precision parameters (equal to the log of the inverse of the variances $\sigma_\varepsilon, \sigma_z$).

For the parameters of the Matérn field, we used penalized complexity (PC) priors (Simpson et al., 2017). PC priors are designed to penalize model complexity and avoid overfitting. For ρ and σ_ω we used the joint PC prior suggested in Fuglstad et al. (2019). The prior parameters are expressed as

$$\text{Prob}(\rho < u_\rho) = \alpha_\rho; \text{Prob}(\sigma_\omega > u_{\sigma_\omega}) = \alpha_{\sigma_\omega},$$

where we set $u_\rho = 700$, $\alpha_\rho = 0.7$, $u_{\sigma_\omega} = 1$ and $\alpha_{\sigma_\omega} = 0.6$. Since the large scale spatial dependence is explained by the

elevation and location covariates, it is reasonable to assume the range of the residual spatial dependence to be smaller than 700 km.

4 | RESULTS

In this section we first look at the residuals of the model given by Equation (2) to check if the assumption of error independence is now more reasonably satisfied. We then discuss parameter estimates for the 24 monthly models and assess model performance through cross-validation. Finally, we use the interpolated monthly surfaces of Tmax and Tmin to calculate climate normals for the following standard 30-year periods: 1961–1990, 1971–2000, 1981–2010 and 1991–2020. A comparison between 1991–2020 and the previous standard periods is then presented.

4.1 | Variograms for the residuals of the spatiotemporal model

The dashed lines in Figure 3 refer to the spatiotemporal variograms for the Tmax residuals of model of Equation (2). The plot shows that the Matérn field allowed to capture the spatiotemporal signal: the

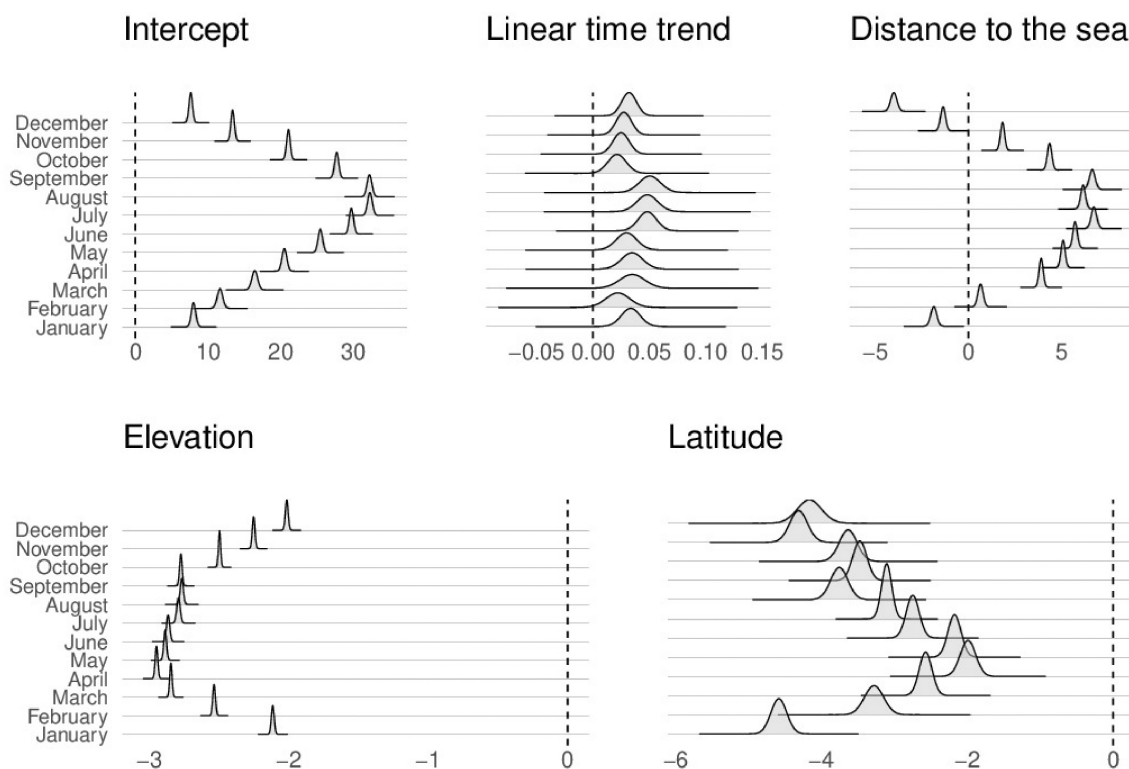


FIGURE 4 Tmax: marginal posterior distributions for the intercept μ , the linear time trend coefficient α and fixed effects β . The shaded colour refers to fixed effects for which the whole 95% credible interval is above or below zero (fixed effects which are significantly different from zero)

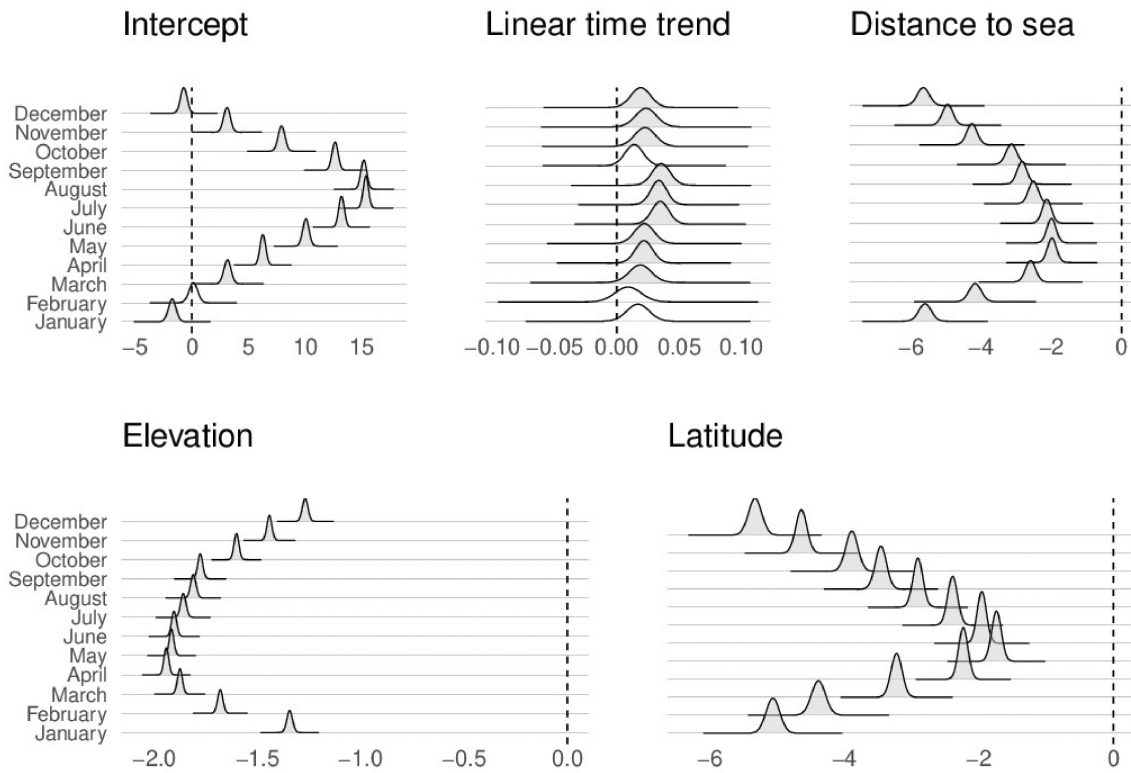


FIGURE 5 T_{min}: marginal posterior distributions for the intercept μ , the linear time trend α and fixed effects β . The shaded colour refers to fixed effects for which the whole 95% credible interval is above or below zero (fixed effects which are significantly different from zero)

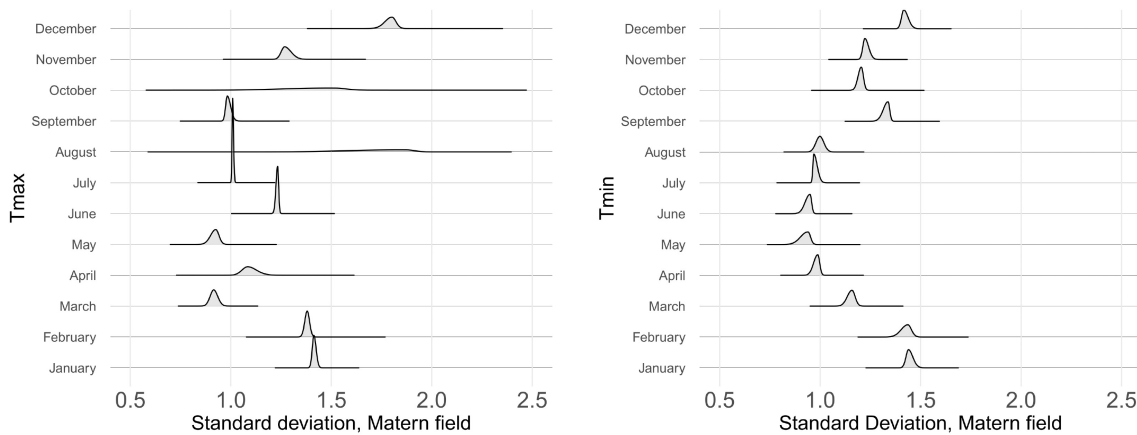


FIGURE 6 Marginal posterior distributions for the standard deviation of the Matérn field $\omega(t,s)$

uncorrelated residuals return variograms which are more or less flat both along the spatial and temporal dimension. This result holds for T_{min} as well (not shown).

4.2 | Parameter estimates

The plots in Figures 4 and 5 reproduce the marginal posterior distributions for the intercept μ , the linear time

effect α and the covariate coefficients β for T_{max} and T_{min} monthly means, respectively.

The plots show both the intercept and the spatial predictors (elevation, latitude and distance to sea) have a clear seasonal behaviour, whatever the parameter (T_{max}/T_{min}). These seasonal-varying effects support our initial hypothesis that a monthly regression analysis could improve the accuracy of the final estimates. Interestingly, both latitude and elevation have a negative

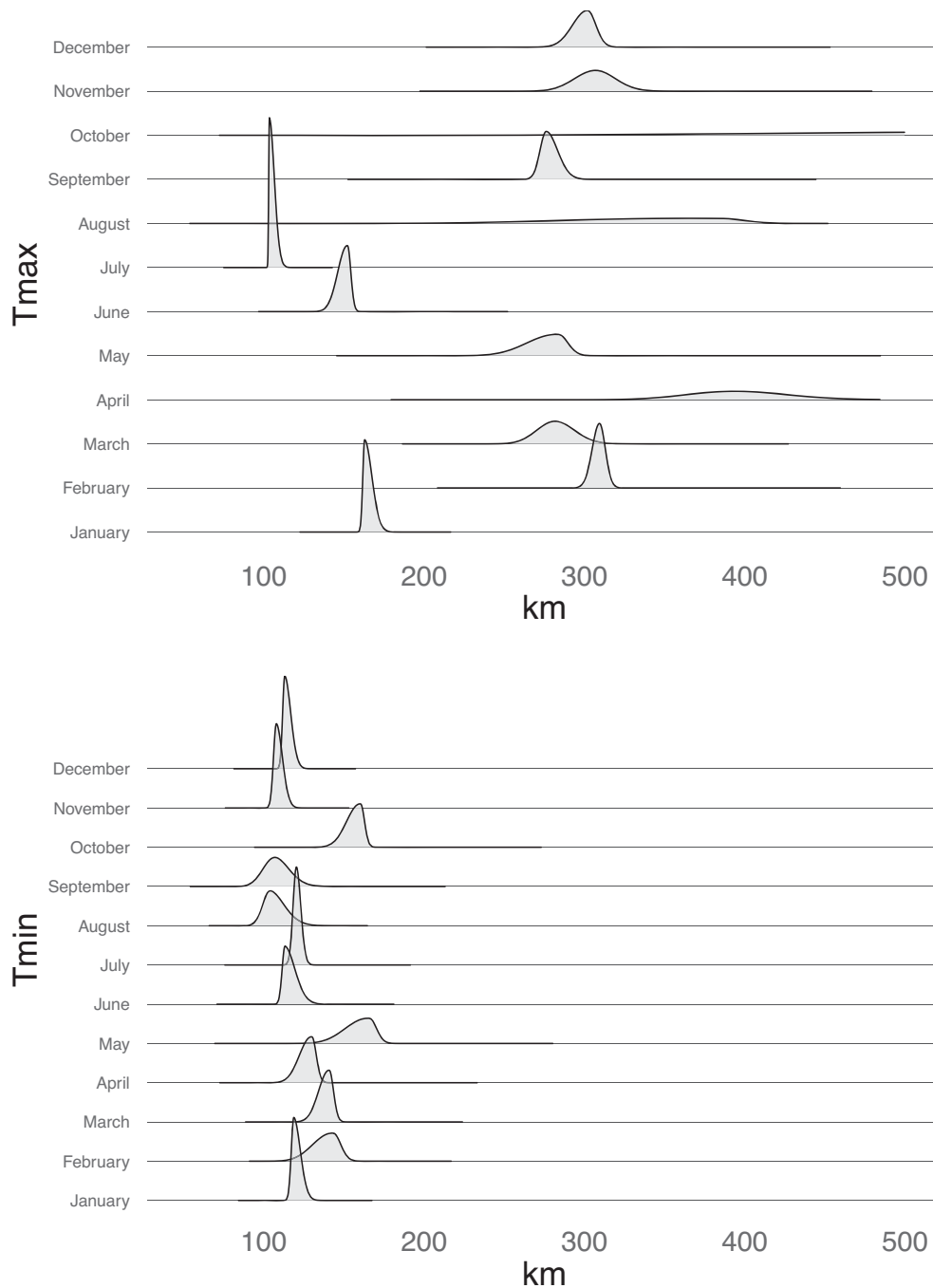


FIGURE 7 Marginal posterior distributions for the spatial range ρ of the Matérn field ω

effect on temperatures across the months, while the sign of the distance to sea effect depends on the variable: when Tmax is considered, distance to sea has a negative effect during the winter season and positive otherwise. Conversely, a negative effect on Tmin monthly means characterizes distance to sea across the year.

The linear time effect α indicates a clear increase of the Tmax and Tmin monthly mean temperatures during 1961–2020, more marked during the summer season (June–August). Further, a significant positive effect characterizes the linear time trend of Tmax across the year,

while a weaker linear time trend effect characterizes the winter season (January and February) and the month of September for Tmin.

The marginal posterior densities of the standard deviation σ_ω and spatial range ρ of the Matérn field ω are reproduced in Figures 6 and 7. As observed above (section 3), the larger ρ is, the more dependent the spatial process is. First, we observe that, unlike the spatial predictors in Figures 4 and 5, here the estimated densities are characterized by very skewed shapes and do not exhibit any pronounced seasonal effect. Second, the

TABLE 1 Cross-validation monthly results: average performance measures over the three validation datasets

	RMSE °C		Correlation		Bias °C	
	Tmax	Tmin	Tmax	Tmin	Tmax	Tmin
January	1.13	1.54	0.96	0.95	0.13	0.02
February	1.05	1.46	0.97	0.95	0.18	0.03
March	1.04	1.36	0.96	0.94	0.23	0.06
April	1.07	1.3	0.96	0.94	0.27	0.11
May	1.15	1.33	0.96	0.94	0.29	0.07
June	1.21	1.48	0.96	0.92	0.29	0.03
July	1.33	1.63	0.95	0.92	0.30	-0.01
August	1.3	1.63	0.95	0.92	0.29	-0.03
September	1.13	1.42	0.96	0.94	0.24	-0.02
October	1.01	1.4	0.97	0.94	0.21	0
November	1	1.37	0.97	0.95	0.15	0.03
December	1.12	1.49	0.97	0.95	0.12	0.04

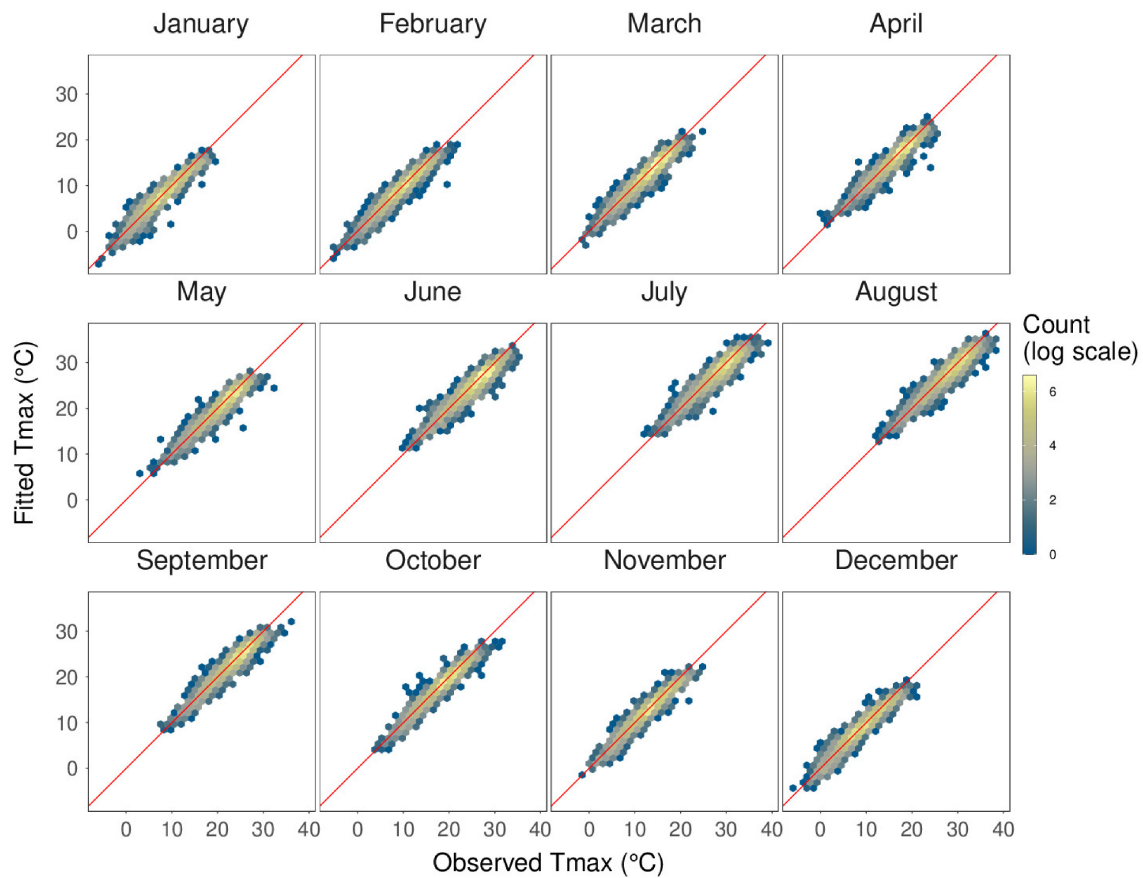


FIGURE 8 Agreement between modelled (means of the posterior predictive distributions) and observed Tmax monthly means. Lighter colours indicate areas with higher points concentrations. The solid line is the 1:1 line as a reference [Colour figure can be viewed at wileyonlinelibrary.com]

visual inspection of the posterior densities suggests that Tmax data show much more spatial structure than Tmin: the posterior mean of ρ varies between 100 and 160 km

for Tmin and between 100 and 500 km for Tmax. At the same time, both the standard deviation and the spatial range of Tmax shows greater variability than Tmin.

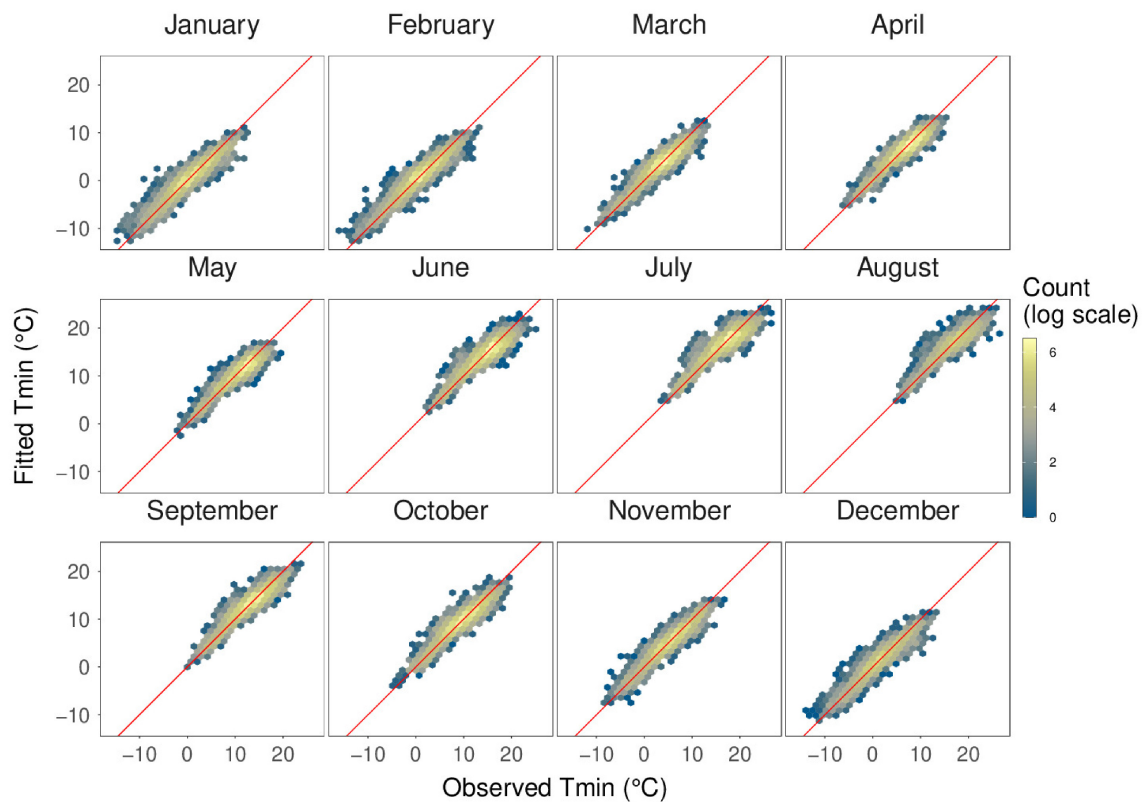


FIGURE 9 Agreement between modelled (means of the posterior predictive distributions) and observed Tmin monthly means. Lighter colours indicate areas with higher points concentrations. The solid line is the 1:1 line as a reference [Colour figure can be viewed at [wileyonlinelibrary.com](https://onlinelibrary.wiley.com/doi/10.1002/joc.8240)]

We conclude this section observing that the estimated densities of the spatial range are consistent with the variograms reproduced in Figure 3 for the residuals of model 1. For example, the diffuse posterior density for the month of October indicates that for Tmax the spatial correlation decays slowly at long distance. Its posterior mean is 488 km and its 95% credible interval is quite wide with bounds of 323 and 616 km. Indeed, the corresponding variograms increase slowly and level off after 250 km (the maximum spatial distance reported in Figure 3). Conversely, the posterior distribution for the month of January is characterized by a posterior mean of 165 km and a narrow 95% credible interval with bounds of 160 and 173 km. A spatial range of approximately 160 km can be inferred by a visual inspection of the variogram of Figure 3.

4.3 | Model validation

To investigate if the model generalizes well or suffers from overfitting/underfitting, we implemented the following validation strategy. First, we identified the weather stations which provide data across all months both for Tmax and Tmin (it can happen that a station does not meet completeness criteria for a specific month and/or variable). These

stations were stratified according to their network of origin (see section 2.2). Within each network, we sampled randomly 10% of the stations in order to define a validation dataset (67 stations). The remainder of the stations constitutes the training dataset. Finally, we fitted the 24 monthly models to the training stations and the fitted models were used to predict the monthly mean temperatures on the validation stations. The above procedure was repeated using three different validation and training datasets.

As performance measures we choose the following statistics comparing predicted and observed values: (1) the Pearson correlation coefficient; (2) the root-mean-square error (RMSE); (3) the bias (calculated as difference between fitted and observed values). For each station, these statistics are computed by comparing the observed Tmax and Tmin monthly means and the means of the corresponding posterior predictive distributions (PPDs; McElreath, 2020) computed using the spatiotemporal model. For each of the three validation datasets, the average of each performance measure over all stations was computed. Table 1 reports the global model performance, that is, the average of each score over the three different validation datasets.

The results of Table 1 suggest a good model performance across the months both for Tmax and Tmin. The Pearson correlation coefficient is always greater than 0.9, while the

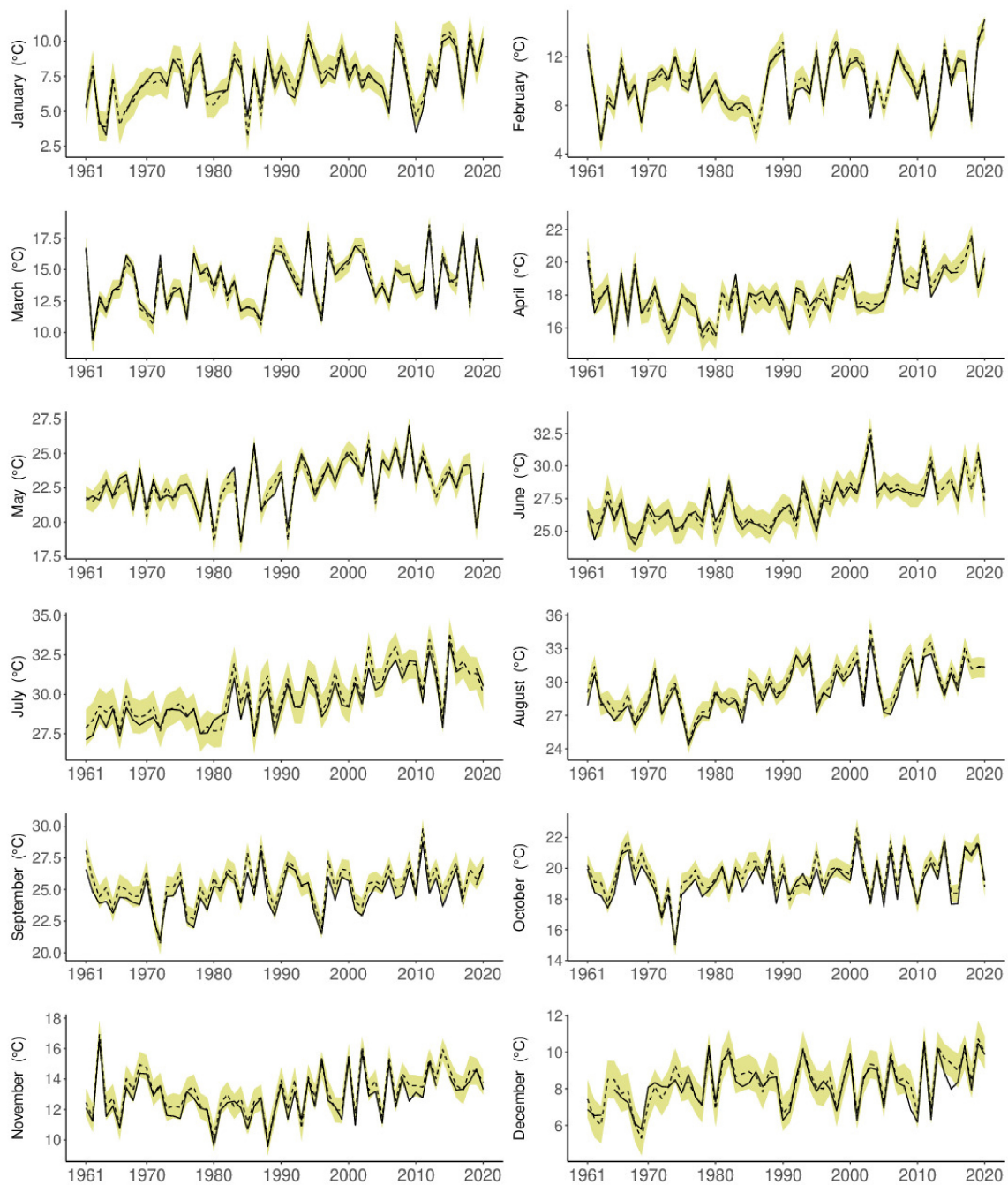


FIGURE 10 Maximum temperature monthly time series for the station of “Forli urbana” (Emilia-Romagna, north of Italy). Observed (solid lines) versus fitted values (dashed lines). The 95% credible interval of each series is represented as a yellow band [Colour figure can be viewed at wileyonlinelibrary.com]

bias ranges between 0 and 0.3°C in absolute value. Finally, the RMSE is always lower than 1.5°C with the exception of the months of January, July and August for Tmin.

The scatterplots in Figures 8 and 9 show, for the validation datasets, the distribution of the fitted values (means of the PPDs) versus the observed values for Tmax and Tmin, respectively. The points spread uniformly along the diagonal line, showing good agreement between observed and modelled data.

Figures 10 and 11 compare observed and predicted annual time series for two illustrative stations chosen from the validation dataset. The plots indicate that the Tmax and Tmin monthly models are able to reproduce the temporal variability of the weather stations in the validation dataset. Each estimate (mean of the PPD) comes with an associated measure of uncertainty: the yellow band marks the bounds of the 95% prediction interval (Figures 10 and 11). In general, almost all of the observed

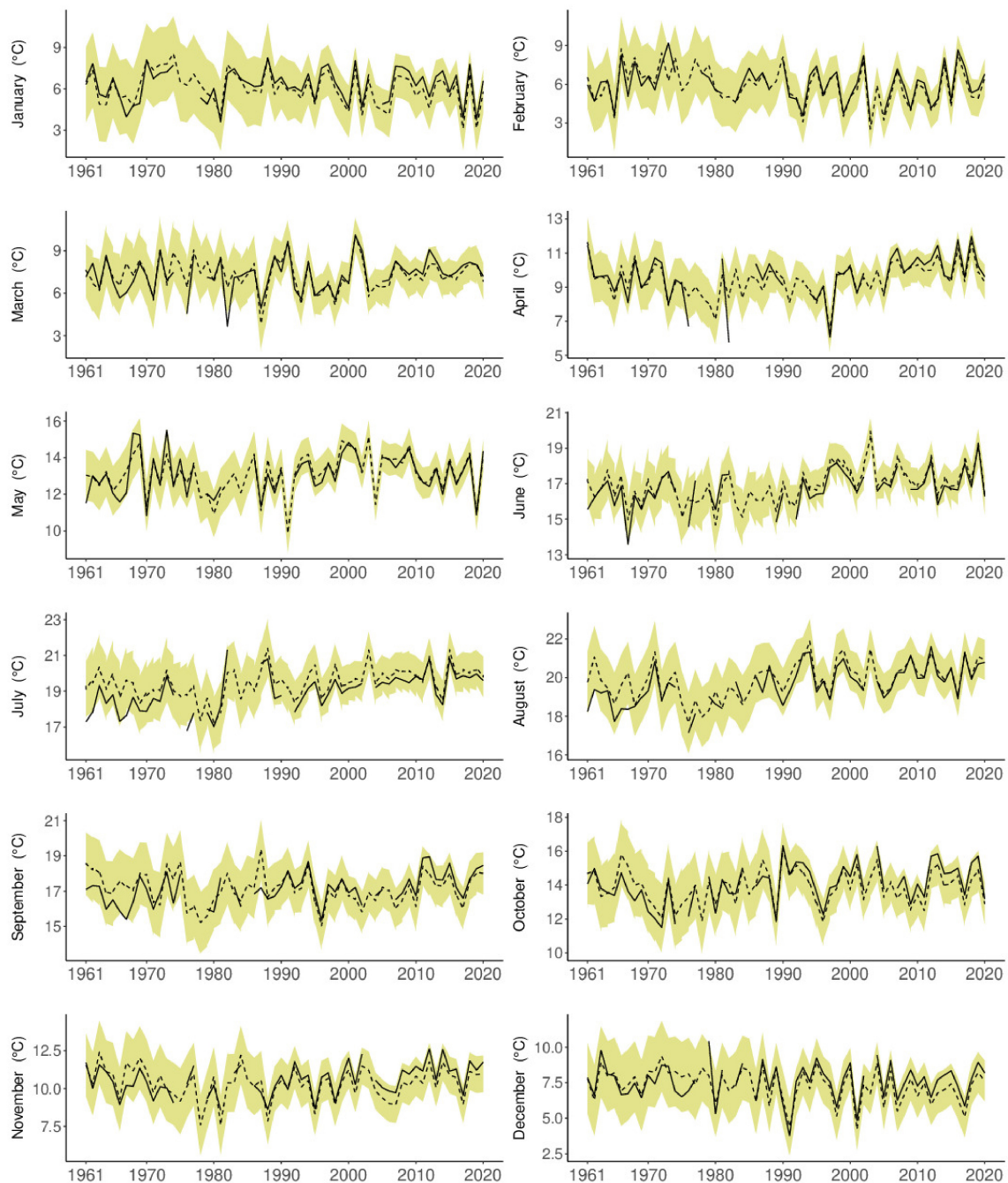


FIGURE 11 Minimum temperature monthly time series for the station of Mileto (Calabria, south of Italy). Observed (solid lines) versus fitted values (dashed lines) [Colour figure can be viewed at wileyonlinelibrary.com]

temperatures fall within their 95% prediction interval. Note, in this example the 95% prediction intervals are quite wide for the station of Mileto in Figure 11.

4.4 | Tmax and Tmin monthly climatologies

Once the model is fitted, it is possible to sample from the posterior distribution of all parameters. Each sample

would correspond to parameters values that are plausible under our model assumptions and observed data. We use such simulated values in order to generate gridded maps of temperatures over the space–time domain considered in the paper: the Italian territory in the period 1961–2020. For each month and year, we generate 1000 such maps. These represent an ensemble that embeds in a natural way the various uncertainties in the model.

We can then use such simulated maps to create 1000 long-term (30-year) monthly averages (climatologies), for

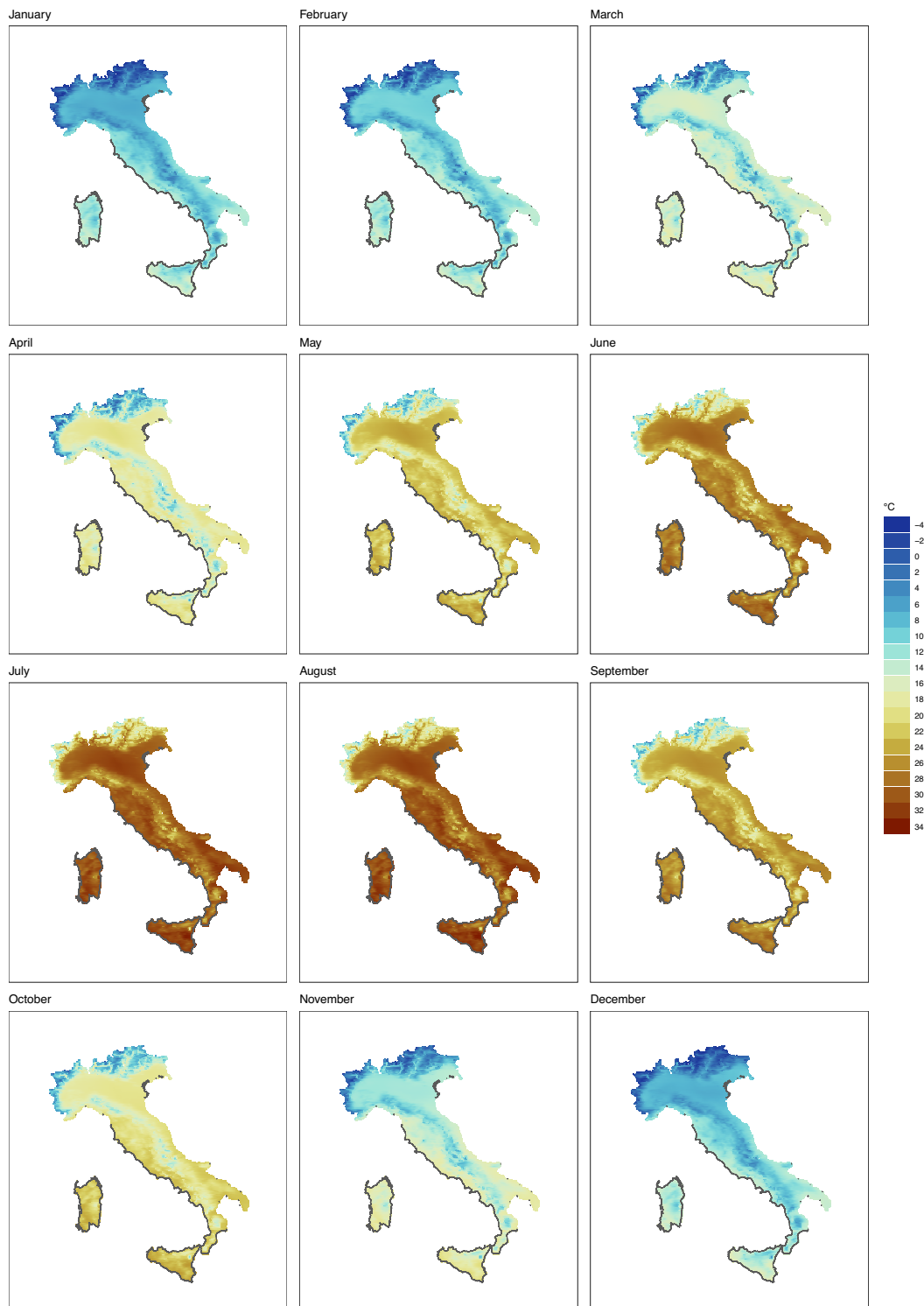


FIGURE 12 Mean of the sample distribution of the monthly climatologies in Italy for the period 1991–2020 (Tmax) [Colour figure can be viewed at wileyonlinelibrary.com]

example, for the period 1991–2020. The 1000 climatologies represent a distribution of gridded maps, which we summarize using their mean and standard deviation. In Figures 12 and 13 the resulting means are plotted for the period 1991–2020 for Tmax and Tmin, respectively.

The corresponding standard deviations maps are in Figure 14 (Tmax only).

These maps point to a global low degree of uncertainty in our predictions, with values of the standard deviation lower than 0.3°C. As expected, greater

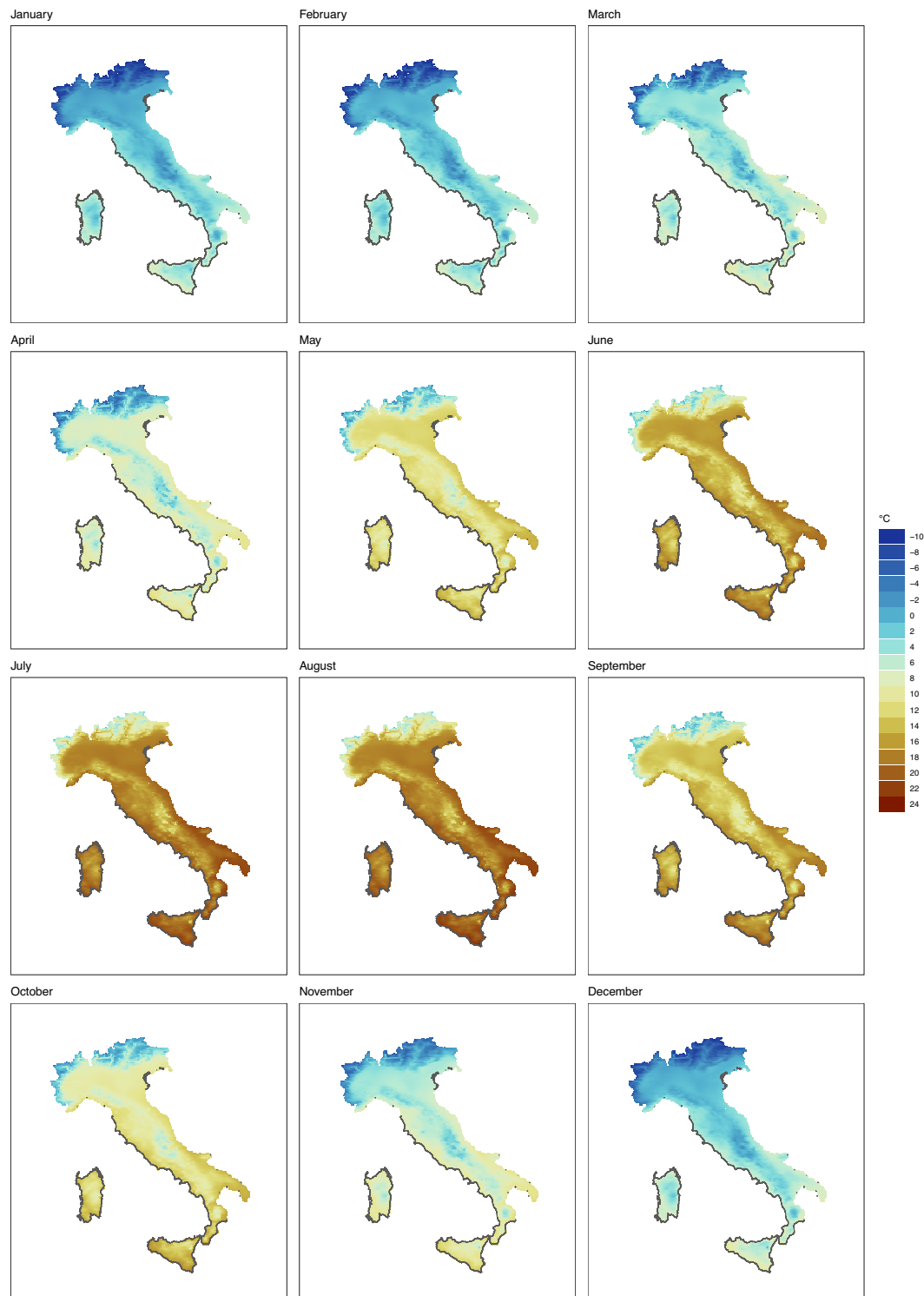


FIGURE 13 Mean of the sample distribution of the monthly climatologies in Italy for the period 1991–2020 (T_{min}) [Colour figure can be viewed at wileyonlinelibrary.com]

uncertainty affects those areas where the density of the weather stations is poorer (see the spatial distribution of the input stations in Figure 1).

Another way to use our ensemble of gridded maps is to compute “difference” maps (1991–2020 vs. 1961–

1990, 1991–2020 vs. 1971–2000, 1991–2020 vs. 1981–2010). We follow the same procedure as before, that is, we compute 1000 differences for each month and year and then summarize them using mean and standard deviation.

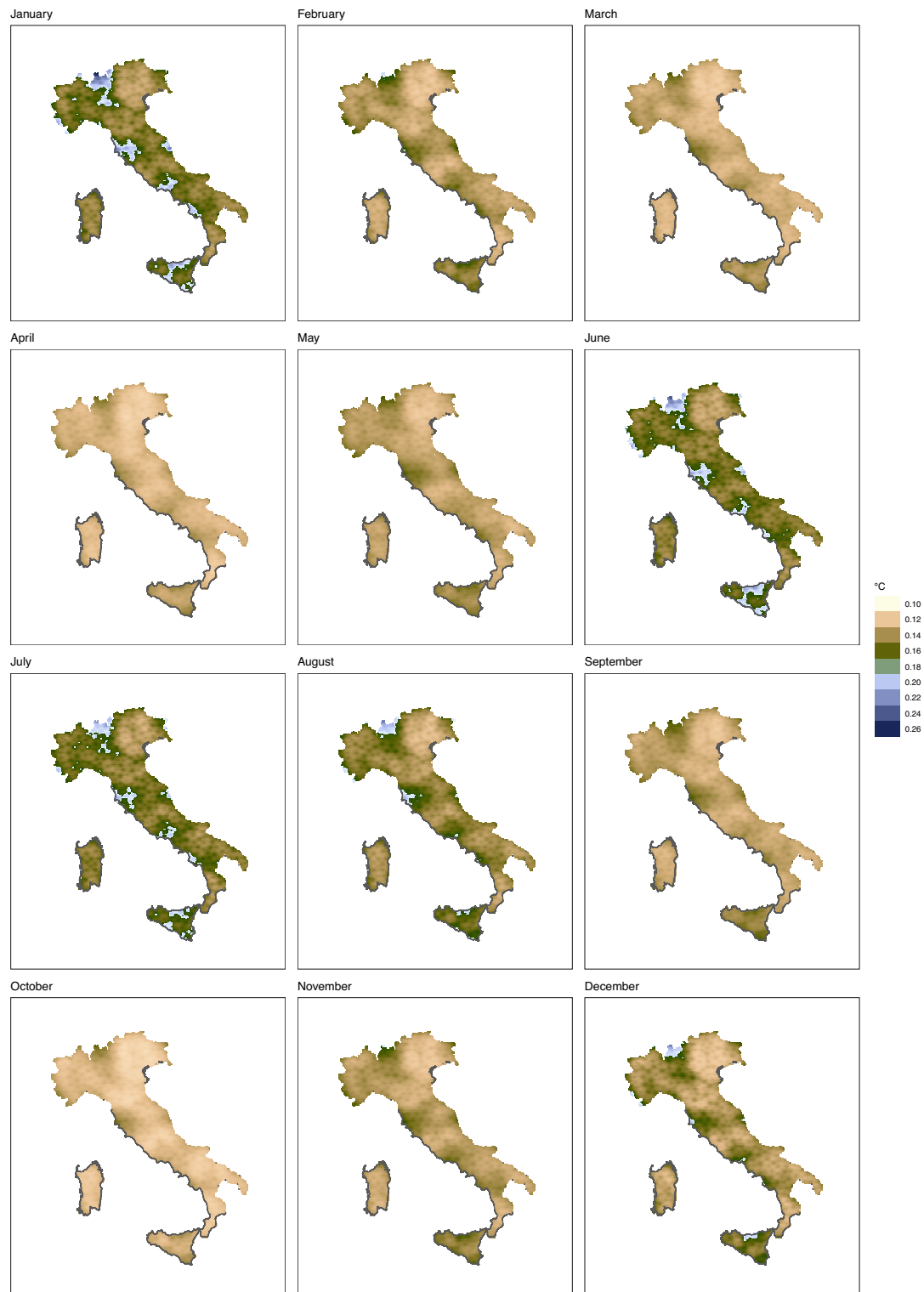


FIGURE 14 Standard deviation maps for the monthly climatologies in Italy for the period 1991–2020 (Tmax) [Colour figure can be viewed at wileyonlinelibrary.com]

Figure 15 displays the mean of such sample distributions. Here, we have used a black contour line to mark those areas where the difference is statistically significant (i.e., the whole 95% credible interval is above or below the zero value). For lack of space, we have

illustrated the difference maps only for Tmax and 1 month per season.

Our results show that the 1991–2020 climatologies are generally warmer than the historical ones in all seasons and regions of Italy. With respect to 1961–1990 and

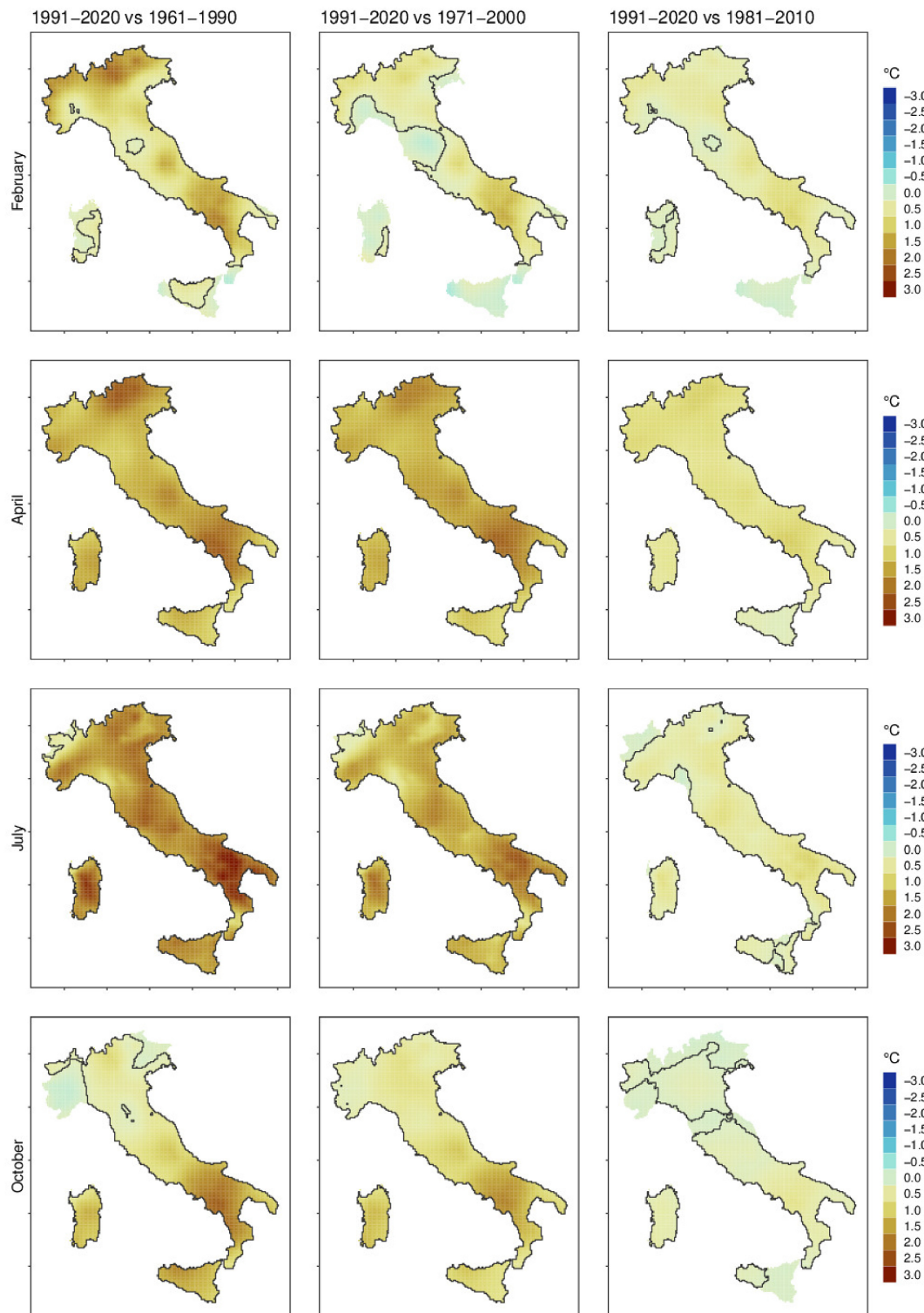


FIGURE 15 Mean of the differences between the monthly 1991–2020 climatology and the historical climatologies: 1961–1990, 1971–2000, 1981–2010 (Tmax). For lack of space, only 1 month per season is represented in the figure. A black contour line marks the areas where the difference is statistically significant from zero [Colour figure can be viewed at [wileyonlinelibrary.com](https://onlinelibrary.wiley.com/doi/10.1002/joc.8240)]

1971–2000, the warming signal seems to be particularly marked in April and July. Notably, in a few areas the 1991–2020 climatologies are somewhat cooler than those calculated for the previous 30-year standard periods (see,

e.g., the negative values which characterize the 1991–2020 vs. 1971–2000 map in February). However, the attached 95% credible interval shows that such negative differences are not statistically significant.

5 | CONCLUSIONS

In this study, we have introduced the INLA-SPDE approach for the interpolation of relevant climate variables. To better illustrate how it works on a real case study, we have implemented a Bayesian regression model for the spatiotemporal interpolation of Tmax and Tmin monthly means during the period 1961–2020. We have used quality controlled and homogenized daily temperature time series from a free and open database. Then, we have generated monthly climate normals of maximum and minimum temperature in Italy for the latest standard 30-year period (1991–2020) and three previous standard ones: 1961–1990, 1971–2000 and 1981–2010.

Since we are mainly interested in the long term trends we have run the regression analysis separately for each month (January–December). This allows to tackle the large space–time domain of our study and avoid the need for a cyclic component that accounts for the yearly seasonality. From a computational point of view, this approach is less demanding than a model where the 12×60 months are jointly modelled. Having 12 independent models also allows to easily account for the changing temperature-versus-predictors relationship.

Our model has a simple formulation. There are three relevant spatial predictors and a linear time effect accounting for the temporal trend in the observed monthly temperatures. Furthermore, a Matérn field allows to capture the residual spatiotemporal correlation. Despite its simplicity, this approach provides a useful and flexible model to produce accurate continuous gridded surfaces equipped with model-based uncertainties. Illustrative examples of the successful use of this model (with only minor modifications) are given in Fioravanti et al. (2021), for the interpolation of PM₁₀ daily concentrations in Italy during 2015, and in Fioravanti et al. (2022), for the assessment of the spatiotemporal variability of NO₂ in Italy during the COVID-19 lockdown.

Classical kriging-based approaches are very common in climate science. However, they fail to incorporate the uncertainty from the spatial covariance matrix into the variance of predicted values. In this regard, Le and Zidek (1992) observed that uncertainty underestimation can result in unwarranted confidence in the interpolated values and, potentially, to unjustified decisions or regulatory actions. Here, we overcome this issue with the use of Bayesian statistics. Our Bayesian model provides a formal approach to handle and propagate uncertainty in the data and in the fitted model parameters. In this regard, we have shown how, through simulation, we are able to generate multiple plausible gridded surfaces of Tmax and Tmin monthly means, which can be further summarized

through measures of central tendency (e.g., posterior mean) or variability (e.g., standard deviation). Following this logic, we have provided examples both of standard deviation maps (to investigate how uncertainty affects our estimates of the 1991–2020 monthly climatologies and where) and 95% credible intervals (to assess the regions where the 1991–2020 period is significantly warmer than the previous 30-year standard periods).

In this work, we use cross-validation as a technique to validate our model. Although this is a very common choice, it is known that cross-validation can be problematic in presence of correlated data (Roberts et al., 2017; Wadoux et al., 2021). Recently, in the INLA framework, a new cross-validation strategy, that takes into account the model structure and the data dependencies, has been proposed by Liu and Rue (2023). This method was not available at the time we prepared this article, but we believe it is an interesting and promising approach that can overcome some of the problems in the common case of cross-validation in presence of correlated data.

Although the mathematics underlying the INLA-SPDE approach may be somewhat intimidating for climate practitioners who are still more familiar with classical geostatistical tools like gstat, the INLA-SDPE approach comes with two user friendly R implementations: the R-INLA and the inlabru package. These packages make the INLA-SPDE methodology a fast, reliable and easy to use tool to scientists with R coding skills, especially if one considers that INLA-SPDE can be also used with non-Gaussian response variables.

The proposed model can be extended in various directions. A first development is to consider a nonlinear time effect in order to accommodate the change-point and the rapid warming in global and European temperature time series from the mid-1970s onward (Toreti & Desiato, 2007). In the current work we have tackled this issue through a random effect $z(t)$ which accounts for the extra temporal variability that is not captured by the linear time trend. An alternative solution offered by R-INLA package is to introduce a smooth component with the use of a random walk model. A more interesting possible development would consist in the use of INLA-SPDE for the integration of in-situ observations and spatially consistent gridded estimates (spatial fusion). A promising solution in this respect has been proposed by Moraga et al. (2017) and, more recently, Wang and Furrer (2021).

6 | CODE AND DATA AVAILABILITY

Our analysis was run using the software package R. The linear model of Equation (1) was fitted with the use of

the *lm* function. The spatiotemporal empirical variograms were calculated using the variogram function of the *gstat* package. This function requires spatiotemporal objects that can be created using the *spacetime* package. For the manipulation of the raster maps we used the *terra* package and the Climate Data Operator (CDO) software (<https://code.mpimet.mpg.de/projects/cdo>). Our plots use scientifically derived colour maps available through the *scico* package (Cramer et al., 2020). The inferential analysis was run using the *inlabru* package (version 2.3.0), an interface for the R-INLA package. To reduce computing time, we enabled the support to the PARDISO library (Alappat et al., 2020; Bollhöfer et al., 2019, 2020). The analysis was run on a workstation with Ubuntu ver. 18.04.6. The running time for each model was of around 20 minutes. Scripts and data used for this study are available on https://github.com/guidofioravanti/climatological_values_inla.

AUTHOR CONTRIBUTIONS

Guido Fioravanti: Conceptualization; methodology; software; data curation; validation; writing – original draft.

Sara Martino: Conceptualization; methodology; formal analysis; writing – original draft; software; validation.

Michela Cameletti: Methodology; writing – review and editing. **Andrea Toreti:** Writing – review and editing; methodology.

ORCID

Guido Fioravanti  <https://orcid.org/0009-0001-6444-8766>

REFERENCES

- Alappat, C.L., Hager, G., Schenk, O., Thies, J., Basermann, A., Bishop, A.R. et al. (2020) A recursive algebraic coloring technique for hardware-efficient symmetric sparse matrix-vector multiplication. *ACM Transactions on Parallel Computing*, 7, 1–37.
- Blangiardo, M. & Cameletti, M. (2015) *Spatial and spatio-temporal Bayesian models with r-inla*. Chichester: John Wiley & Sons.
- Bollhöfer, M., Eftekhari, A., Scheidegger, S. & Schenk, O. (2019) Large-scale sparse inverse covariance matrix estimation. *SIAM Journal on Scientific Computing*, 41, A380–A401. Available from: <https://doi.org/10.1137/17M1147615>
- Bollhöfer, M., Schenk, O., Janalik, R., Hamm, S. & Gullapalli, K. (2020) *State-of-the-art sparse direct solvers*. Cham: Springer, pp. 3–33. Available from: https://doi.org/10.1007/978-3-030-43736-7_1
- Bruley, E., Mouillot, F. & Lauvaux, T. (2022) Enhanced spring warming in a Mediterranean mountain by atmospheric circulation. *Scientific Reports*, 12, 7721.
- Brunetti, M., Maugeri, M., Nanni, T., Simolo, C. & Spinoni, J. (2014) High-resolution temperature climatology for Italy: interpolation method intercomparison. *International Journal of Climatology*, 34, 1278–1296.
- Caloiero, T., Coscarelli, R. & Pellicone, G. (2020) A gridded database for the spatiotemporal analysis of rainfall in southern Italy (Calabria region). *Environmental Sciences Proceedings*, 2, 6.
- Chen, S. & Guo, J. (2017) Spatial interpolation techniques: their applications in regionalizing climate-change series and associated accuracy evaluation in northeast China. *Geomatics, Natural Hazards and Risk*, 8, 689–705.
- Cornes, R.C., van der Schrier, G., van den Besselaar, E.J.M. & Jones, P.D. (2018) An ensemble version of the E-OBS temperature and precipitation data sets. *Journal of Geophysical Research: Atmospheres*, 123, 9391–9409.
- Cos, J., Doblas-Reyes, F., Jury, M., Marcos, R., Bretonnière, P.-A. & Samsó, M. (2022) The Mediterranean climate change hotspot in the CMIP5 and CMIP6 projections. *Earth System Dynamics*, 13, 321–340.
- Cramer, F., Shephard, G. & Heron, P. (2020) The misuse of colour in science communication. *Nature Communications*, 11, 5444.
- Crespi, A., Matiu, M., Bertoldi, G., Petitta, M. & Zebisch, M. (2021) A high-resolution gridded dataset of daily temperature and precipitation records (1980–2018) for trentino-south tyrol (northeastern Italian Alps). *Earth System Science Data*, 13, 2801–2818.
- Curci, G., Guijarro, J.A., Di Antonio, L., Di Bacco, M., Di Lena, B. & Scorzini, A.R. (2021) Building a local climate reference dataset: application to the abruzzo region (central Italy), 1930–2019. *International Journal of Climatology*, 41, 4414–4436.
- Daly, C., Gibson, W.P., Taylor, G.H., Johnson, G.L. & Pasteris, P. (2002) A knowledge-based approach to the statistical mapping of climate. *Climate Research*, 22, 99–113.
- Desiato, F., Fioravanti, G., Frascchetti, P., Perconti, W. & Toreti, A. (2011) Climate indicators for Italy: calculation and dissemination. *Advances in Science and Research*, 6, 147–150.
- Durre, I., Menne, M., Gleason, B., Houston, T. & Vose, R. (2010) Comprehensive automated quality assurance of daily surface observations. *Journal of Applied Meteorology and Climatology*, 49, 1615–1633.
- Fang, S., Mao, K., Xia, X., Wang, P., Shi, J., Bateni, S.M. et al. (2022) Dataset of daily near-surface air temperature in China from 1979 to 2018. *Earth System Science Data*, 14, 1413–1432.
- Fioravanti, G., Cameletti, M., Martino, S., Cattani, G. & Pisoni, E. (2022) A spatiotemporal analysis of NO₂ concentrations during the Italian 2020 COVID-19 lockdown. *Environmetrics*, 33, e2723.
- Fioravanti, G., Martino, S., Cameletti, M. & Cattani, G. (2021) Spatiotemporal modelling of PM₁₀ daily concentrations in Italy using the SPDE approach. *Atmospheric Environment*, 248, 118192.
- Fioravanti, G., Piervitali, E. & Desiato, F. (2019) A new homogenized daily data set for temperature variability assessment in Italy. *International Journal of Climatology*, 39, 5635–5654.
- Fuglstad, G.-A., Simpson, D.P., Lindgren, F. & Rue, H. (2019) Constructing priors that penalize the complexity of Gaussian random fields. *Journal of the American Statistical Association*, 114, 445–452.
- GCOS. (2017) *Indicators of climate change. Outcome of a meeting held at WMO 3 February 2017*. Geneva: GCOS. Technical report.
- Gelfand, A.E., Diggle, P.J., Fuentes, M. & Guttorp, P. (2010) *Handbook of spatial statistics*. Boca Raton, FL: Chapman and Hall/CRC.
- Guijarro, J. (2019) *climatol: Climate Tools (Series Homogenization and Derived Products)*.
- Handcock, M.S. & Stein, M.L. (1993) A Bayesian analysis of kriging. *Technometrics*, 35, 403–410.

- Helbert, C., Dupuy, D. & Carraro, L. (2009) Assessment of uncertainty in computer experiments from universal to Bayesian kriging. *Applied Stochastic Models in Business and Industry*, 25, 99–113.
- Herrera, S., Kotlarski, S., Soares, P.M.M., Cardoso, R.M., Jaczewski, A., Gutiérrez, J.M. et al. (2019) Uncertainty in gridded precipitation products: influence of station density, interpolation method and grid resolution. *International Journal of Climatology*, 39, 3717–3729. Available from: <https://doi.org/10.1002/joc.5878>
- Hofstra, N., Haylock, M., New, M., Jones, P. & Frei, C. (2008) Comparison of six methods for the interpolation of daily, European climate data. *Journal of Geophysical Research: Atmospheres*, 113, D21110.
- ISPRA. (2016) *Controlli di qualità delle serie di temperatura e precipitazione*. Roma: ISPRA. Technical report.
- ISPRA. (2021) *Gli indicatori del clima in Italia nel 2020—anno xvi*. Roma: ISPRA. Technical report. Available from: <https://www.isprambiente.gov.it/resolueuid/611cf5c4734448639d24a3b8ff32b90d>
- Joelsson, L.M.T., Sturm, C., Södling, J., Engström, E. & Kjellström, E. (2022) Automation and evaluation of the interactive homogenization tool homer. *International Journal of Climatology*, 42, 2861–2880.
- Le, N.D. & Zidek, J.V. (1992) Interpolation with uncertain spatial covariances: a Bayesian alternative to kriging. *Journal of Multivariate Analysis*, 43, 351–374.
- Ledesma, J.L. & Futter, M.N. (2017) Gridded climate data products are an alternative to instrumental measurements as inputs to rainfall-runoff models. *Hydrological Processes*, 31, 3283–3293.
- Lian, X., Zeng, Z., Yao, Y., Peng, S., Wang, K. & Piao, S. (2017) Spatiotemporal variations in the difference between satellite-observed daily maximum land surface temperature and station-based daily maximum near-surface air temperature. *Journal of Geophysical Research: Atmospheres*, 122, 2254–2268.
- Libertino, A., Ganora, D. & Claps, P. (2018) Technical note: space-time analysis of rainfall extremes in Italy: clues from a reconciled dataset. *Hydrology and Earth System Sciences*, 22, 2705–2715.
- Lindgren, F., Bolin, D. & Rue, H. (2022) The SPDE approach for Gaussian and non-Gaussian fields: 10 years and still running. *Spatial Statistics*, 50, 100599.
- Lindgren, F. & Rue, H. (2015) Bayesian spatial modelling with R-INLA. *Journal of Statistical Software*, 63, 1–25.
- Lindgren, F., Rue, H. & Lindström, J. (2011) An explicit link between Gaussian fields and Gaussian Markov random fields: the stochastic partial differential equation approach. *Journal of the Royal Statistical Society Series B (Statistical Methodology)*, 73, 423–498.
- Lionello, P. & Scarascia, L. (2018) The relation between climate change in the Mediterranean region and global warming. *Regional Environmental Change*, 18, 1481–1493.
- Liu, Z. & Rue, H. (2023) Leave-group-out cross-validation for latent Gaussian models.
- Lo Papa, G., Dazzi, C., Némethy, S., Corti, G. & Cocco, S. (2020) Land set-up systems in Italy: a long tradition of soil and water conservation sewed up to a variety of pedo-climatic environments. *Italian Journal of Agronomy*, 15, 281–292.
- Maechler, M., Rousseeuw, P., Struyf, A., Hubert, M. & Hornik, K. (2021) cluster: Cluster Analysis Basics and Extensions. R package version 2.1.1—for new features, see the “Changelog” file (in the package source). Available from: <https://CRAN.R-project.org/package=cluster>
- Martino, S. & Riebler, A. (2020) Integrated nested Laplace approximations (INLA). In: Balakrishnan, N., Colton, T., Everitt, B., Piegorsch, W., Ruggeri, F. & Teugels, J.L. (Eds.) *Wiley statsRef: statistics reference online*. Hoboken, NJ: John Wiley & Sons, Ltd. Available from: <https://doi.org/10.1002/9781118445112.stat08212>
- Masson-Delmotte, V., Zhai, P., Pirani, A., Connors, S., Péan, C., Berger, S. et al. (2021) *IPCC 2021: summary for policymakers. Climate change 2021: the physical science basis. Contribution of working group I to the sixth assessment report of the Intergovernmental Panel on Climate Change*. Cambridge and New York, NY: IPCC.
- McElreath, R. (2020) *Statistical rethinking. A Bayesian course with examples in R and Stan*. Boca Raton, FL: CRC Press.
- Menne, M., Durre, I., Vose, R., Gleason, B. & Houston, T. (2012) An overview of the global historical climatology network-daily database. *Journal of Atmospheric and Oceanic Technology*, 29, 897–910.
- Merchant, C.J., Paul, F., Popp, T., Ablain, M., Bontemps, S., Defourny, P. et al. (2017) Uncertainty information in climate data records from earth observation. *Earth System Science Data*, 9, 511–527.
- Moraga, P., Cramb, S.M., Mengersen, K.L. & Pagano, M. (2017) A geostatistical model for combined analysis of point-level and area-level data using inla and spde. *Spatial Statistics*, 21, 27–41.
- Moyeed, R. & Papritz, A. (2002) An empirical comparison of kriging methods for nonlinear spatial point prediction. *Mathematical Geology*, 34, 365–386.
- My, L., Di Bacco, M. & Scorzini, A.R. (2022) On the use of gridded data products for trend assessment and aridity classification in a mediterranean context: the case of the apulia region. *Water*, 14, 2203.
- Nature. (2019) Scientific uncertainty. *Nature Climate Change*, 9, 797.
- Osborn, T.J., Jones, P.D., Lister, D.H., Morice, C.P., Simpson, I.R., Winn, J.P. et al. (2021) Land surface air temperature variations across the globe updated to 2019: the CRUTEM5 data set. *Journal of Geophysical Research: Atmospheres*, 126, e2019JD032352.
- Pastor, F., Valiente, J.A. & Khodayar, S. (2020) A warming Mediterranean: 38 years of increasing sea surface temperature. *Remote Sensing*, 12, 2687.
- Pebesma, E.J. (2004) Multivariable geostatistics in s: the gstat package. *Computers & Geosciences*, 30, 683–691.
- Pellicone, G., Caloiero, T., Modica, G. & Guagliardi, I. (2018) Application of several spatial interpolation techniques to monthly rainfall data in the Calabria region (southern Italy). *International Journal of Climatology*, 38, 3651–3666.
- Pilz, J., Pluch, P. & Spöck, G. (2005) Bayesian kriging with lognormal data and uncertain variogram parameters. In: *Geostatistics for environmental applications*. Berlin-Heidelberg: Springer, pp. 51–62.
- R Core Team. (2021) *R: a language and environment for statistical computing*. Vienna: R Foundation for Statistical Computing. Technical report. Available from: <https://www.r-project.org/>
- Rantanen, M., Karpechko, A.Y., Lipponen, A., Nordling, K., Hyvärinen, O., Ruosteenoja, K. et al. (2022) The arctic has warmed nearly four times faster than the globe since 1979. *Communications Earth & Environment*, 3, 168.
- Raymond, F., Ullmann, A., Camberlin, P., Drobinski, P. & Smith, C.C. (2017) Extreme dry spell detection and climatology over the Mediterranean basin during the wet season. *Geophysical Research Letters*, 43, 7196–7204.
- Roberts, D.R., Bahn, V., Ciuti, S., Boyce, M.S., Elith, J., Guiller-Arroita, G. et al. (2017) Cross-validation strategies for data with

- temporal, spatial, hierarchical, or phylogenetic structure. *Ecography*, 40, 913–929. Available from: <https://doi.org/10.1111/ecog.02881>
- Rue, H., Martino, S. & Chopin, N. (2009) Approximate Bayesian inference for latent Gaussian models using integrated nested Laplace approximations (with discussion). *Journal of the Royal Statistical Society Series B*, 71, 319–392.
- Sahu, S. (2021) *Bayesian modeling of spatio-temporal data with R*. New York: Chapman and Hall/CRC.
- Serrano-Notivol, R., Beguera, S. & de Luis, M. (2019) Stead: a high-resolution daily gridded temperature dataset for Spain. *Earth System Science Data*, 11, 1171–1188.
- Simpson, D.P., Rue, H., Riebler, A., Martins, T.G. & Sørbye, S.H. (2017) Penalising model component complexity: a principled, practical approach to constructing priors. *Statistical Science*, 32, 1–28.
- Song, J., Kwon, S. & Lee, G. (2015) Incorporation of parameter uncertainty into spatial interpolation using Bayesian trans-Gaussian kriging. *Advances in Atmospheric Sciences*, 32, 413–423.
- Spano, D., Mereu, V., Bacciu, V., Marras, S., Trabucco, A., Adinolfi, M. et al. (2020) *Analisi del rischio. i cambiamenti climatici in Italia*. Lecce: CMCC. Technical report.
- Tang, G., Clark, M.P. & Papalexiou, S.M. (2022) EM-earth: the ensemble meteorological dataset for planet earth. *Bulletin of the American Meteorological Society*, 103, E996–E1018.
- Tarek, M., Brissette, F. & Arsenault, R. (2021) Uncertainty of gridded precipitation and temperature reference datasets in climate change impact studies. *Hydrology and Earth System Sciences*, 25, 3331–3350.
- Toreti, A. & Desiato, F. (2007) Changes in temperature extremes over Italy in the last 44 years. *International Journal of Climatology*, 2(28), 733–745.
- Toreti, A., Kuglitsch, F.G., Xoplaki, E., Della-Marta, P.M., Aguilar, E., Prohom, M. et al. (2011) A note on the use of the standard normal homogeneity test to detect inhomogeneities in climatic time series. *International Journal of Climatology*, 31, 630–632.
- Tuel, A. & Eltahir, E.A.B. (2020) Why is the Mediterranean a climate change hot spot? *Journal of Climate*, 33, 5829–5843.
- Wadoux, A.M.-C., Heuvelink, G.B., de Bruin, S. & Brus, D.J. (2021) Spatial cross-validation is not the right way to evaluate map accuracy. *Ecological Modelling*, 457, 109692.
- Wang, C. & Furrer, R. (2021) Combining heterogeneous spatial datasets with process-based spatial fusion models: a unifying framework. *Computational Statistics and Data Analysis*, 161, 107240.
- Wikle, C., Zammit-Mangion, A. & Cressie, N. (2019) *Spatio-temporal statistics with R*. Boca Raton, FL: Chapman and Hall/CRC.
- WMO. (2017) *WMO guidelines on the calculation of climate normals*. Geneva: World Meteorological Organization. Technical report.
- WMO. (2021) *State of the global climate 2020*. Geneva: World Meteorological Organization. Technical report.
- Yang, R. & Xing, B. (2021) A comparison of the performance of different interpolation methods in replicating rainfall magnitudes under different climatic conditions in Chongqing province (China). *Atmosphere*, 12, 1618.
- Zittis, G., Almazroui, M., Alpert, P., Ciaia, P., Cramer, W., Dahdal, Y. et al. (2022) Climate change and weather extremes in the eastern Mediterranean and middle east. *Reviews of Geophysics*, 60, e2021RG000762.
- Zittis, G., Hadjinicolaou, P. & Klängidou, M. (2019) A multi-model, multi-scenario, and multi-domain analysis of regional climate projections for the Mediterranean. *Regional Environmental Change*, 19, 2621–2635.
- Zuur, A.F., Ieno, E.N. & Elphick, C.S. (2010) A protocol for data exploration to avoid common statistical problems. *Methods in Ecology and Evolution*, 1, 3–14.

How to cite this article: Fioravanti, G., Martino, S., Cameletti, M., & Toreti, A. (2023). Interpolating climate variables by using INLA and the SPDE approach. *International Journal of Climatology*, 43(14), 6866–6886. <https://doi.org/10.1002/joc.8240>